Dielectrophoretic Handling of Mesoscopic Objects

Diego C. POLITANO, Paolo V. PRATI, Shao-Jü WOO,
Otte J. HOMAN *), Felix M. MOESNER and Andreas STEMMER

Institute of Robotics, Nanotechnology Group
*) Laboratory of Fieldtheory and Microwave Electronics

Swiss Federal Institute of Technology Zurich (ETHZ)
CH - 8092 Zurich, Switzerland

ABSTRACT

Efficient handling of minute objects in individual or collective mode is a delicate and most demanding task. Electric fields applied over a micro-patterned electrode array possess the capability to produce contactless driving forces on small conducting or non-conducting particles as presented in a former paper [1]. The transport and precise positioning of charged micro particles up to 400 µm in diameter has been demonstrated on the x-y plane, where an addressable electrode geometry allows flexible particle actuation trajectories.

In this paper, the electrode pattern is further miniaturized allowing a gap width in the order of a 1 µm. The advantage of this downscaling is a clear reduction of Coulomb heating when small objects are transported in ionic solution. Additionally, high frequency electric fields are necessary to impart actuation forces onto the suspended objects in liquid environment as described in [2 - 4]. Since the electric field strength is a function of the gap between the electrodes and the applied voltage, a miniaturized pattern requires lower voltage amplitudes in order to attain a certain electric field strength.

The electrodes are designed as a spiraled meander and fabricated by photolithographic processes within a monolayer. Under the application of six-phase voltages, a traveling electric field wave is created above the electrode array, immersed mesoscopic objects become polarized and negative dielectrophoretic effects cause object motion. It is shown that optimal object actuation occurs in a narrow, material-specific frequency spectrum. Various simulations and their results are presented in this paper.

I. INTRODUCTION

A particle suspended in a medium becomes electrically polarized when subjected to an electric field. If the spatial distribution of phase and field magnitude are inhomogenous, a dielectrophoretic (DEP) force acts on the particle, as a result of the interactions between the induced polarization and the field. The DEP-induced particle motion is strongly dependent on the field frequency, the spatial configuration of the field, the dielectric properties of the suspending medium and, more importantly, of the particle itself.

II. THEORETICAL BACKGROUND

The term dielectrophoresis was coined by Pohl [5] to describe the force exerted by a non-uniform electric field on a small polarized but uncharged particle. Most theoretical and experimental work in dielectrophoresis used the generally accepted force expression of Pohl [5], namely

$$\overrightarrow{F_{DEP}} = \left(\overrightarrow{p_{eff}} \cdot \nabla\right) \cdot \vec{E}_o \qquad (1)$$

where $\overrightarrow{E_0}$ is the non-uniform electric field and $\overrightarrow{p_{eff}}$ is the effective dipole moment to be discussed in more detail in this paper. The simplest derivation of the dielectrophoretic force is accomplished by summing the forces on two equal but opposite electric charges (+q,-q) placed a vector distance $\vec{d}$ apart in a non-uniform electric field (see Fig. 1).

The net force $\overrightarrow{F_{DEP}}$ on this small dipole is given as [6]

$$\overrightarrow{F_{DEP}} = q \cdot \vec{E}_o \cdot (\vec{r} + \vec{d}) - q \cdot \vec{E}_o \cdot \vec{r} \quad . \qquad (2)$$

If $\vec{d} \to 0$ and only the lowest-order term of the Taylor series in $\vec{d}$ is retained, we get

$$\overrightarrow{F_{DEP}} = q \cdot (\vec{d} \cdot \nabla) \cdot \vec{E}_o \quad . \qquad (3)$$

The product ($q\vec{d}$) is interpreted as an electric dipole $\vec{P}$, so we have [5, 6]:

$$\overrightarrow{F_{DEP}} = \left(\overrightarrow{p_{eff}} \cdot \nabla\right) \cdot \vec{E_o} \tag{4}$$

where [7]

$$\overrightarrow{p_{eff}} = 4\pi a^3 \varepsilon_m \frac{(\varepsilon_p - \varepsilon_m)}{(\varepsilon_p + 2\varepsilon_m)} \vec{E_o} \tag{5}$$

is the value of the induced dipole moment. Here, a is the distance between the two charges and the dielectric constants of the media and the particle are ε_m and ε_p, respectively.

We modified this situation considering the general case, where the field varies sinusoidally in time and where both particle and suspending medium possess a finite conductivity (σ_p and σ_m respectively). The absolute permittivity is then a complex quantity, having real and imaginary components given by

$$\varepsilon^* = \varepsilon - j\left(\frac{\sigma}{\omega}\right) \tag{6}$$

where $j = \sqrt{-1}$ and ω is the angular frequency. We should note that the permittivity factor ε_m outside the brackets of Eq. (5) derives from the Gauss law and as such is not considered to include the effect of conductivity losses. Now, the induced dipole is given by [7, 8] as

$$\overrightarrow{p_{eff}} = 4\pi a^3 \varepsilon_m \frac{(\varepsilon_p{}^* - \varepsilon_m{}^*)}{(\varepsilon_p{}^* + 2\varepsilon_m{}^*)} \vec{E_o} \quad . \tag{7}$$

We can finally go back to Eq. (4) and find that the dielectrophoretic force $\overrightarrow{F_{DEP}}$ acting on a particle in a non-uniform traveling field is composed of two components.

The first one is the "in-phase" component (conventional dielectrophoresis):

$$\overline{F_{CDEP}} = 2\pi a^3 \varepsilon_m \Re e\left(\frac{(\varepsilon_p{}^* - \varepsilon_m{}^*)}{(\varepsilon_p{}^* + 2\varepsilon_m{}^*)}\right) \nabla \bar{E}^2 \tag{8}$$

whereas the second one is the "out-of-phase" component (traveling wave dielectrophoresis) [9]:

$$\bar{F}(\omega) = \frac{-4\pi^2 a^3 \varepsilon_m \Im m\left(\frac{(\varepsilon_p{}^* - \varepsilon_m{}^*)}{(\varepsilon_p{}^* + 2\varepsilon_m{}^*)}\right) \bar{E}^2}{\lambda} \tag{9}$$

where λ is the wavelength of the traveling field and

$$f_{CM} = \frac{(\varepsilon_p{}^* - \varepsilon_m{}^*)}{(\varepsilon_p{}^* + 2\varepsilon_m{}^*)} \tag{10}$$

the so-called Clausius-Mossotti factor.

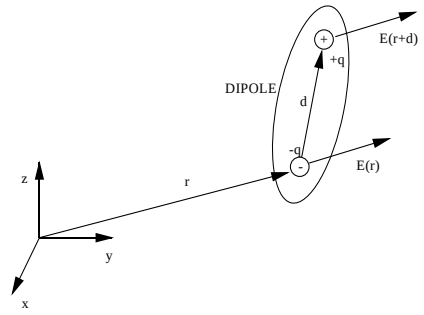

FIGURE 1: Dipole in non-uniform electric field as shown in Cartesian xyz system.

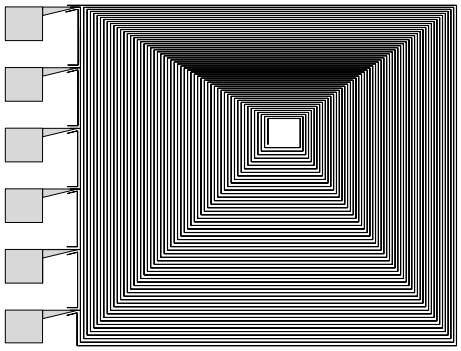

FIGURE 2: Magnified design of the electrode pattern SNAIL. Six-phase voltages are supplied to the pads on the left side. The constant electrode gaps differ for each of the four quadrants.

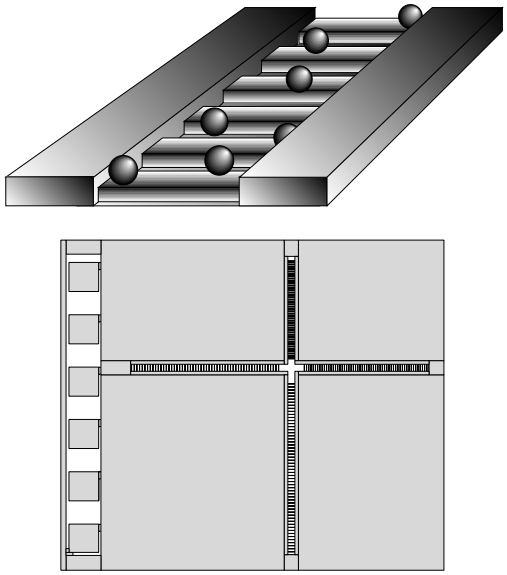

FIGURE 3: Micro channels covering the electrode meander structure. The channels have the function of guiding the particles and serve as a reference for observation under the microscope.

In conclusion, we find the final expression for the dielectrophoretic force referring back to [9] as

$$\bar{F}(\omega) = 2\pi a^3 \varepsilon_m \left(Re(f_{CM}) \nabla \bar{E}^2 + Im(f_{CM}) \left(E_x^2 \nabla \varphi_x + E_y^2 \nabla \varphi_y + E_z^2 \nabla \varphi_z \right) \right) \quad (11)$$

III. Electrode Pattern

The electrodes are designed as a spiraled meander and consequently named as SNAIL. We previously demonstrated that the best translation results have been achieved with six-phase electrodes [10 - 12]. Now, the novel miniaturized structure consists of six parallel electrodes designed as shown in Fig. 2. Every side of the structure features a different gap width between the electrodes resulting in 4 segments with different electric field strength. The electrical contact to the power supply is provided by large pads which also provide for impedance transformation from the microelectrodes to the supply wires.

The structure SNAIL is fabricated by photolithographic processes within a monolayer and is then – as an alternative – covered by a thin isolation film. On each side, only few microchannels (Fig. 3) are designed, where the particle interacts directly with the electrodes. These channels function as a guidance for the particles and as reference for the observation under the light microscope.

The electrode-free window in the middle of the structure is designed for statistical measurements and for further applications such as optical-tweezer (laser-trapping) methods.

The microelectrodes are fabricated on glass or Indiumphosphide (InP) substrate. Using optical photolithography, patterns with a minimum linewidth of 1µm are defined. Samples are produced as a single layer of gold metallization using a Galvanic process. Some critical spots for the fabrication process are shown in Fig. 4.

IV. Mesoscopic Particles & Suspending Media

The mesoscopic particles used in later experiments are Latex (Polystyrene) spheres with a diameter d = 1 µm, mass density ρ = 1,05 g/ml, dielectric constant ε = 2.5 and electrical conductivity σ_p = 0.009 S/m (Ernest F. Fullam, pdf@fullam.com).

The suspending medium is water with some Ethanol which acts as bacteria-killer. The dielectric constant is ε = 80 and the electrical conductivity $\sigma_m = 5\ 10^{-6}$ S/m

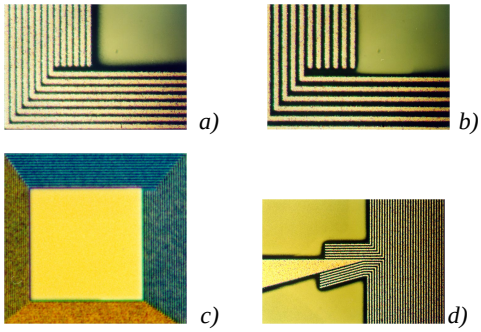

FIGURE 4: Magnified view of the critical points of the electrode pattern. *a)* and *b)* show central termination of electrodes; *c)* is the central window; *d)* is the pad connection to one phase electrode.

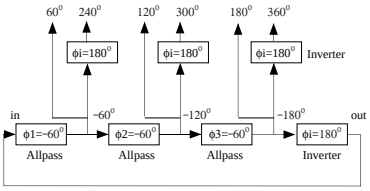

FIGURE 5: Block diagramm of the six-phase oscillator.

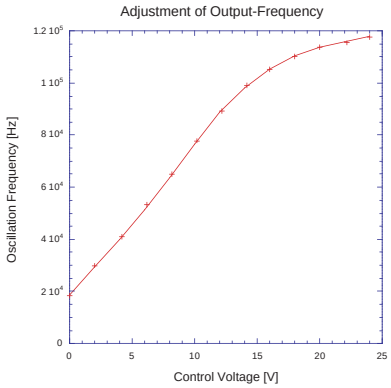

FIGURE 6: Output frequency vs. controlling dc voltage of the sine quadrature VCO.

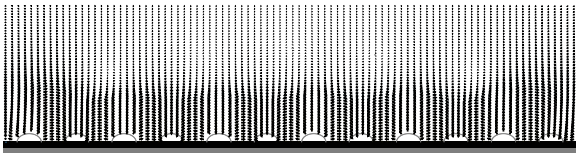

FIGURE 7: Two-phase field distribution over the SNAIL electrode array.

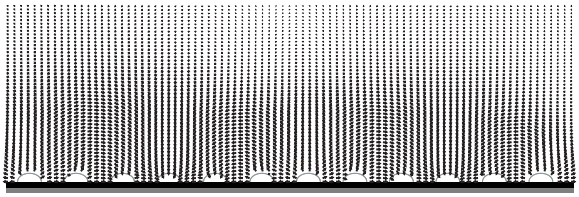

FIGURE 8: Six-phase field distribution over the SNAIL electrode array.

which can be raised up to 10 S/m by addition of salt resulting in an ionic solution.

V. Power Supply

Quadrature generators producing two signals of identical frequency and amplitude but different phase angle are used in a variety of applications and described in [13].

We have further enhanced this technique in order to build a generator that produces 6 signals of identical frequency and amplitude. In this case, the frequency shift is 60^o.

The circuit utilizes 3 allpass filters with a 60^o shift and 4 inverters as shown in Fig. 5. As long as the inverter stage does not add any additional phase error (ϕ_i = 180^o) the sum of the allpass stages must amount to $\phi_1+\phi_2+\phi_3+\phi_4+\phi_5 = 180^o$ for oscillation.

The frequency can be tuned with a VCO working between 0 and 25V DC. A frequency range from 20 MHz up to 119 MHz can be covered as shown in Fig. 6.

VI. Simulations

vi.i. Electric Field Distribution on the SNAIL

In order to reach the maximal traveling effect on the particle, we tried to optimize it through the electrode stimulation. The electric field distribution on the SNAIL was investigated by various simulations with the program tool MMP (Multiple Multipole) developed at ETH-Zurich by Dr. Pascal Leuchtmann [14]. The results of our simulations are summarized in the two figures Fig. 7 and Fig. 8.

In Fig. 7, a two-phase distribution was simulated. This solution was adopted in a previous research [7]. The field distribution shows the abrupt transition between different phases; so that we can postulate that this solution can't assure a perfect control on the moving particles.

We have further simulated the six-phase setup. Fig. 8 shows its field distribution on the SNAIL. The transitions are much smoother. Therefore, this solution was chosen as it assures good particle moving control.

Further, the influence of the particle on the local field distribution was also investigated. As shown in the theory, the local non-uniformity of the field is a decisive parameter in the dielectric force calculation (see Eq. (8)). Fig. 9 shows a representation of the distribution of E^2 near the electrode in presence of a particle.

Fig. 10 shows the potential distribution on the electrodes. The graph clearly indicates the reduction of the magnitude for greater height above the electrodes.

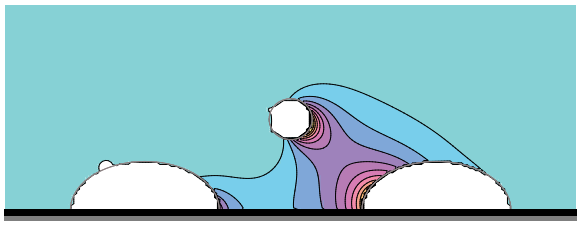

FIGURE 9: The representation of the E^2 distribution showing the particle influence within the local field.

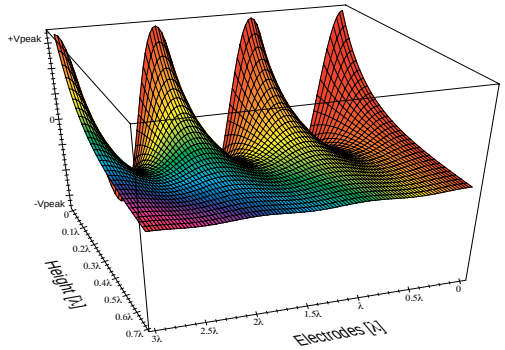

FIGURE 10: The picture shows the potential distribution on the electrodes. The magnitude becomes reduced for greater height above the electrodes.

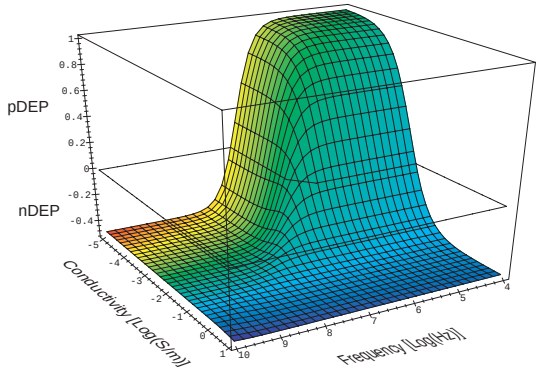

FIGURE 11: Real part of f_{CM} in function of frequency and medium conductivity σ_m.

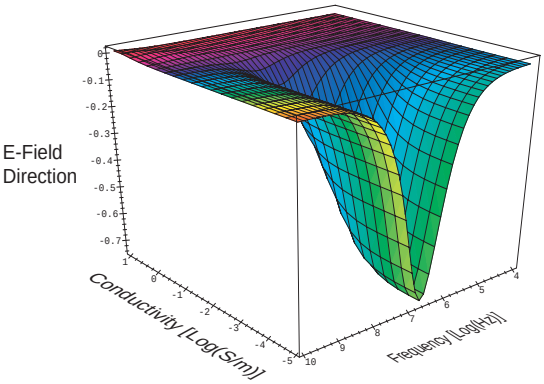

FIGURE 12: Imaginary part of f_{CM} in function of frequency and medium conductivity σ_m.

vi.ii. The Influence of the Clausius-Mossotti Factor

In this paper, the influence of the Clausius-Mossotti factor is investigated with respect to some critical particle handling consequences. Starting from the representation of the real part (Fig. 11) and the imaginary part (Fig. 12) of the Clausius-Mossotti factor f_{CM}, we found the interesting result shown in Fig. 13. The conventional dielectrophoresis (cDEP) causes trapping or repulsion from the electrode, while only the imaginary component (traveling wave dielectrophoresis, twDEP) is responsible for particle translational motion. Fig. 13 states that the best frequency spectrum is between 10 MHz and 100 MHz, where cDEP is negative and causes repulsion from the electrodes, and where the magnitude of twDEP is big enough to induce a motion on the particle.

From the results shown in Fig. 13, we can postulate the feasibility of sorting particles with different dielectric properties or dimensions (e.g. separating living from not living cells) [15].

It is now possible to calculate the speed of a particle on the fabricated electrode pattern. If the Stokes friction force is

$$\vec{W}_R = -6\pi\eta a \cdot \vec{v} \tag{12}$$

with η as the viscosity and $\vec{v}$ as the motion velocity. Together with the twDEP force

$$\vec{F}_{twDEP} = 2\pi a^3 \Im m(f_{CM})\left(E^2_{xo}\nabla\phi_x + E^2_{yo}\nabla\phi_y + E^2_{zo}\nabla\phi_z\right) \tag{13}$$

we assume that

$$E^2_{xo}\nabla\phi_x + E^2_{yo}\nabla\phi_y + E^2_{zo}\nabla\phi_z = \overline{E^2}\cdot\frac{2\pi}{\lambda} \tag{14}$$

so we find

$$\vec{F}_{twDEP} = \overrightarrow{-W_R} \tag{15}$$

$$\frac{-4\pi^2 a^3 \varepsilon_m \Im m(f_{CM})\big|_{\omega = 9MHz}\ \bar{E}^2}{\lambda} = 6\pi\eta a \bar{v}_{twDEP} \tag{16}$$

and finally, the particle velocity in translational x-direction as

$$\bar{v}_{cDEPx} = \frac{r^2 \varepsilon_m}{3\eta}\Re e(f_{CM})\big|_{\omega = 80MHz}\ \nabla E^2_x \tag{17}$$

VII. Conclusion

From a theoretical point of view, the traveling electric field induces a complex dipole moment on a suspended particle. As a result, a complex dielectrophoretic force is exerted on it. The real component of this force causes trapping while the imaginary component is responsible for translational particle actuation. The overall electrokinetic behavior of a particle is determined by combined effects of these two forces, and is a function of its dielectric properties and the frequency of the applied traveling field. It is shown that optimal actuation occurs in a narrow, material-specific frequency spectrum. Further, the interesting possibility of particle sorting is postulated. The field-induced forces increase as field gradients become stronger. An increase of field gradients can be obtained by a further miniaturization of the electrodes. From a technical point of view, electrodes with typical dimensions in the submicron range can be fabricated with existing photolithographic technologies.

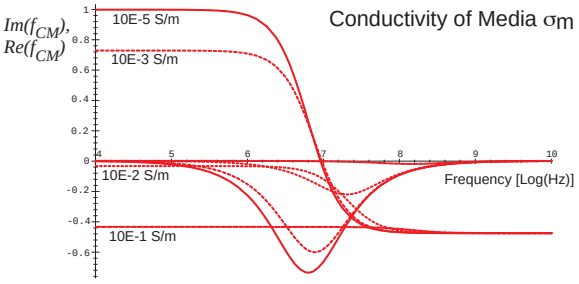

FIGURE 13: Optimal actuation occurs in a narrow, material-specific frequency spectrum.

VIII. Acknowledgments

We thank Mr. S. Müller (Institute of Robotics, ETH Zurich) for his excellent work on the six-phase voltage oscillator. His great engagement in this project allows us to conduct many important experiments in the near future.

IX. References

1. **Moesner**, F.M., **Higuchi**, T., *"Devices for Particle Handling by an AC Electric Field,"* Proceedings IEEE Micro Electro Mechanical Systems, Amsterdam, The Netherlands, January 1995, pp. 66-71.

2. **Muller**, T., **Gerardino**, A., **Schnelle**, T., **Shirley**, S.G., **Bordoni**, F., **De-Gasperis**, G., **Leoni**, R., **Fuhr**, G., *"Trapping of Micrometer and Sub-Micrometer Particles by High-Frequency Electric Fields and Hydrodynamic Forces,"* Journal of Physics D (Applied Physics), vol. 29, no. 2; February 1996, pp. 340-349.

3. **Jones**, T.B., **Washizu**, M. *"Multipolar Dielectrophoretic and Electrorotation Theory,"* Journal of Electrostatics, vol. 37, no.1-2, May 1996, pp. 121-134.

4. **Fuhr** G., **Hagedorn** R., **Müller** T., "*Linear Motion of Dielectric Particles and Living Cells in Microfabricated Structures induced by Traveling Electric Fields*", IEEE MEMS, 1991, pp. 259-264.
5. **Pohl** H.A., " *Dielectrophoresis*", Cambridge University Press, Cambridge, 1978.
6. **Jones** T.B., **Kallio** G.A., "*Dielectrophoretic Force Calculation*", Journal of Electrostatics 6, 1979, pp. 207-224.
7. **Pethig** R., "*Application of AC electrical fields to the manipulation and characterisation of cells*", Proc. of the 4th Toyota Conf., 1990, pp. 159-185.
8. **Washizu** M., "*Manipulation of Biological Objects in Micromachined Structures*", IEEE MEMS, 1992, pp. 196-201.
9. **Huang** Y., **Wang** X.B., **Tame** J.A., **Pethig** R., J Phys. D: Appl Phys. 26, 1993, pp.1528-1535.
10. **Moesner** F.M, **Higuchi** T., "*Devices for Particle Handling by an AC Electric Field*", Proceedings IEEE Micro Electro Mechanical Systems, Amsterdam, The Netherlands, January 1995, pp.66-71.
11. **Moesner** F.M., **Buehler** Ph.S., **Politano** D.C., **Prati** P.V., "*Electrostatic Propulsion Motor for Tiny Vessels*", IEEE Industry Applications Society Conference Record, 32nd Annual Meeting, New Orleans, October 1997, vol.3, pp1874-1878.
12. **Moesner** F.M, **Higuchi** T., "*Contactless Manipulation of Microparts by Electric Field Traps*", SPIE's International Symposium on Microrobotic and Microsystem Fabrication, Pittsburg, October 1997, vol.3202, pp. 168-175.
13. **Hölzel** R., "*A Simple Wide-Band Sine Wave Quadrature Oscillator*", IEEE Transactions on Instrumentation and Measurement, Amsterdam, February 1993, Volume 42, pp.758-760.
14. **Leuchtmann** P., **Bomholt** F., "*Field modeling with the MMP-code*", IEEE Transactions on Electromagnetic Compatibility, 1993. Special issue on EMC applications of numerical techniques.
15. **Talary** M.S., **Burt** J.P.H., **Tame** J.A., **Pethig** R., "*Electromanipulation and separation of cells using traveling electric fields*", J Phys. D: Appl Phys. 29, 1996, pp.2198-2203.